




Enhancing corrosion resistance of 316L stainless steel through electrochemical deposition of polyaniline coatings in acidic environments

Mohammad Fatahiamirdehi², Mohamad Mahani², Seyyedeh Forough Mirseyed³, Auref Rostamian⁴, and Mehdi Ostadhassan^{1,*} 

¹ Institute of Geosciences, Marine and Land Geomechanics and Geotectonics, Christian-Albrechts-Universität, 24118 Kiel, Germany

² Department of Chemistry, Faculty of Chemistry and Chemical Engineering, Graduate University of Advanced Technology, Kerman, Iran

³ Chemistry Institute, University of Campinas (UNICAMP), PO Box 6154, Campinas, SP 13083-970, Brazil

⁴ CEPETRO/FEM - University of Campinas (UNICAMP), 6052, Campinas, SP 13083-970, Brazil

Received: 9 February 2024

Accepted: 21 July 2024

Published online:
30 July 2024

© The Author(s), 2024

ABSTRACT

Stainless steel is widely used because of its excellent corrosion resistance in typical environments. However, it is susceptible to corrosion in acidic media, therefore, to address this issue, the electrochemical deposition of polyaniline coatings on 316L stainless steel was investigated using cyclic voltammetry at different potential windows and scan rates. The successful polymerization and surface morphology were analyzed using Fourier transform infrared spectroscopy (FTIR) and scanning electron microscopy (SEM), respectively. Moreover, thermal stability of the PANI coating was assessed through thermo gravimetric analysis while the corrosion behavior of bare and coated steels immersed in 1M H₂SO₄ was studied using electrochemical impedance spectroscopy (EIS). Based on the Nyquist plots obtained from the EIS revealed that the corrosion resistance of the PANI coating improved significantly with a decrease in scan rate and by limiting the upper potential, especially during longer exposure times up to 72 h. Results suggest that controlling the deposition parameters and optimizing the electrochemical conditions can lead to even greater improvements in the corrosion resistance of the stainless steel. These findings offer valuable insights for researchers and engineers in the field of materials science and corrosion protection, enabling them to develop more precise and efficient strategies for enhancing the durability and performance of stainless steel in acidic environments.

Handling Editor: Zhao Shen.

Address correspondence to E-mail: mehdi.ostadhassan@ifg.uni-kiel.de

Introduction

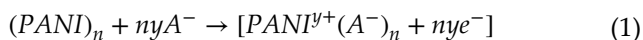
In recent years, organic coatings have been predominantly employed to protect steel alloys, including stainless steels. Stainless steels are widely utilized across various industries due to their exceptional corrosion resistance. One particular stainless-steel variant, known as 316L, exhibits remarkable corrosion resistance owing to the presence of chromium and molybdenum elements [1]. However, it is important to highlight that in highly corrosive environments, the application of 316L stainless steel without implementing preventive measures such as coatings or corrosion inhibitors may not be economically viable [2]. Chromium compounds, which can be utilized as both coatings and inhibitors, have been utilized to effectively reduce the corrosion rate of stainless steels. Nevertheless, it is crucial to acknowledge that these materials possess carcinogenic substances and contribute to environmental pollution. Chromium compounds have been explored as a promising coating material due to their ability to enhance corrosion resistance. For instance, [3] investigated the high-temperature steam oxidation behavior of steels with varying chromium content. Their findings demonstrated that a higher chromium content led to the formation of a superior protective chromia layer, significantly improving corrosion resistance. In a separate study, [4] examined the growth behavior of the chromium-zirconium interlayer in a chromium-coated zirconium alloy exposed to high-temperature steam. Their research revealed a transformation of the interlayer over time, transitioning from a simple parabolic growth to a complex duplex structure and ultimately fragmenting into intertwined zirconium oxide and metallic chromium due to increasing oxygen pressure. These studies highlight the potential of chromium compounds in creating protective coatings and their influence on the material's response to harsh environments.

Due to limitations associated with traditional methods like chemical inhibitors, the use of organic coatings is rapidly growing. Unlike inhibitors, polymeric coatings offer clear advantages. They are easier to apply to surfaces, pose minimal health risks due to their non-toxic nature, and have a reduced environmental footprint. For instance, [5] demonstrated the effectiveness of a two-layer composite coating for magnesium alloy. This coating, comprised of nanoflower-shaped zinc phosphate bonded to a micro-arc oxidation layer, exhibited exceptional

superhydrophobicity and corrosion resistance even under harsh conditions like salt, acid, and sunlight exposure. This example highlights the remarkable potential of organic coatings as a superior alternative for protecting materials.

The concept of employing conductive polymers for corrosion protection was first proposed by MacDiarmid in 1985 [6]. Subsequent research has extensively explored the application of conductive polymers as protective coatings, demonstrating their exceptional corrosion resistance [7–10]. These conductive polymers can be synthesized through chemical or electrochemical methods [11, 12]. Experimental results have revealed that when polyaniline (PANI) is synthesized on steel, it effectively protects the substrate in corrosive environments, even in the presence of strong acids [13–15]. The protection mechanisms of conductive polymers have been attributed to various theories [16]. Firstly, conductive polymers generate an electric field on the metal surface, impeding the flow of electrons from the metal to the oxidizing agent. Secondly, conductive polymers create a dense and low-porosity film on the metal surface, acting as a barrier between the metal and the corrosive environment. Lastly, conductive polymers facilitate the formation of a protective layer of metal oxide on the metal surface. Another advantage of polymeric coatings is their ability to passivate pinholes, further enhancing corrosion protection. Additionally, studies have demonstrated that conductive polymers, when removed from a solution and subsequently re-immersed after drying, can regain their original mechanical and electrical properties without significant deterioration [17].

Conductive polymers can be synthesized using a variety of methods, including chemical polymerization, electrochemical polymerization, photochemical polymerization, plasma polymerization, and solid-state polymerization. Of these methods, electrochemical polymerization is the most widely used due to its simplicity and ability to control the thickness of the polymer film. Among these methods, the electrochemical approach has gained significant attention due to its simplicity and the ability to control the thickness of the polymer film [18]. Furthermore, in the electrochemical polymerization process, dopant ions in the form of cations and anions can be added. Aniline, for instance, undergoes polymerization along with the insertion of anions (dopants) derived from the acid, as depicted by Eq. (1) [19].



The doping degree (y) represents the ratio between the number of charges in the polymer and the number of monomer units. Various factors influence the electrochemical polymerization of aniline using cyclic voltammetry, including the substrate material, scan rate, potential window, number of cycles, dopant anions, electrolyte composition, pH, and others. The corrosion of stainless steel in acidic environments can lead to significant economic losses, safety hazards, and environmental concerns. By investigating the effectiveness of polyaniline coatings, this study aims to provide a potential solution to mitigate corrosion and extend the lifespan of stainless steel components. The objective of the present study is to investigate the corrosion behavior of polyaniline (PANI) coatings on 316L stainless steel, synthesized using cyclic voltammetry. Specifically, we aim to explore the influence of scan rate and potential window during the cyclic voltammetry process on the properties of the PANI coating.

Experimental methods and samples

The substrate utilized in this study was 316L stainless steel, with an area of 0.78 cm^2 . The chemical composition of the stainless-steel substrate is provided in Table 1. Prior to the experiments, the specimens were meticulously polished using up to 2400-grit SiC (silicon carbide) abrasive paper, followed by $1 \mu\text{m}$ diamond paste, to achieve a smooth surface. Subsequently, the specimens were thoroughly degreased using acetone to remove any residual contaminants. Aniline and sulfuric acid, both of which were obtained from Merck (Darmstadt, Germany), were employed in the experimental procedures. Aniline, prior to its use, underwent a distillation process and was stored in a dark and cool environment to preserve its quality. It is essential to perform the distillation operation to eliminate impurities such as hydroquinone and other phenolic compounds, which could interfere with or even halt the polymerization process. To ensure complete extraction of aniline, the distillation process was performed twice, further guaranteeing the purity of the reagent.

The deposition of PANI coatings was accomplished using a solution comprising $0.1 \text{ M H}_2\text{SO}_4$ with 0.1 M aniline through the cyclic voltammetry technique involving 10 cycles. The potential cycling ranged from -0.1 V to 1.4 V /AgCl for sample 1. The specific potential windows employed during the cyclic voltammetry process were as follows: -0.2 V – 1.4 V for the first cycle, 0.1 V – 1 V for the second cycle, and 0.1 V – 0.9 V for subsequent cycles in the case of sample 2. Notably, within these potential ranges, only the formation of a passive layer occurs without the polymerization of the monomer. For the deposition process, a three-electrode cell configuration was utilized. The working electrode consisted of stainless steel 316L, the reference electrode was Ag/AgCl, and Pt served as the counter electrode (as illustrated in Fig. 1). Electrochemical investigations were performed using an Autolab PGSTAT 302N system (Metrohm, Utrecht, Netherlands).

To investigate the impact of scan rate during the polymerization process on the corrosion behavior, two different scan rates were employed: 10 mV/s (low scan rate) and 50 mV/s (high scan rate). The sample preparation conditions are summarized in Table 2.

To ensure successful polymerization of aniline and to characterize the resulting thin film, Fourier-transform

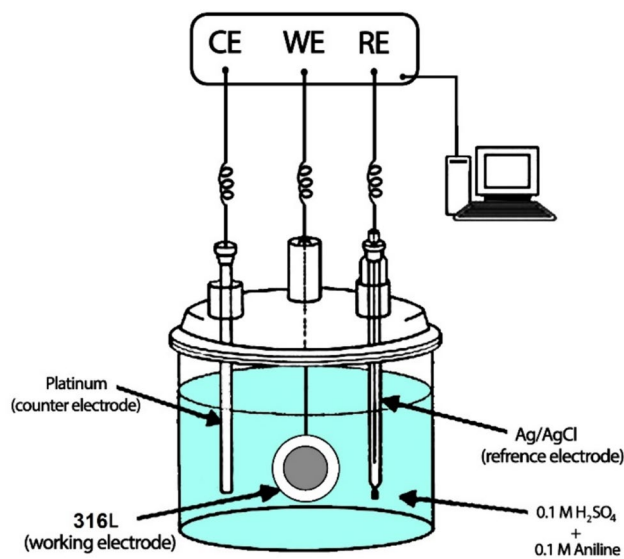


Figure 1 Schematic set up of electrochemical cell.

Table 1 Chemical composition of the 316L stainless steel

C%	Ni%	Si%	Mn%	P%	S%	Cr%	Mo%	Fe%
0.027	10.28	0.42	1.62	0.031	0.018	17.12	1.9	Balance

Table 2 Sample preparation conditions

Sample	Scan rate (mV/s)	Potential window
S ₁	10	−0.1–1.4 V
S ₂	10	−0.2–1.4 V, 0.1–1 V, 0.1–0.9 V
S ₃	50	−0.1–1.4 V

infrared (FTIR) spectroscopy was performed using a Vectory22 instrument (Bruker Optics, Karlsruhe, Germany) in the wavenumber range of 500–2000 cm^{−1}. Electrochemical impedance spectroscopy (EIS) was employed to assess the corrosion behavior of both coated and bare steel specimens immersed in 1 M H₂SO₄ for varying durations. The Nyquist plots were recorded within a frequency range of 100 kHz–1 mHz, with an amplitude of 10 mV. The impedance data were analyzed using ZSimpWin 3.30 software. To gain a comprehensive understanding of the effectiveness and durability of the polyaniline (PANI) coatings, further analysis was conducted on the bare and coated steel samples after 72 hrs. of immersion. Scanning electron microscopy (SEM) was employed using a STOE STADI-MP instrument from Germany to examine the morphology of the samples. This technique allowed for a detailed examination of the surface characteristics and the presence of any corrosion-related features. By comparing the electron micrographs of the bare steel samples with those of the coated ones, it was possible to visually assess the protective properties of the PANI coatings and identify any signs of corrosion or degradation.

Furthermore, the thermal stability of the PANI coatings was evaluated using thermogravimetric analysis (TG). This technique measures the weight changes of the coatings as they are subjected to increasing temperatures. By analyzing the TG data, it was possible to determine the temperature at which the coatings start to degrade or lose their protective properties. This information is crucial in understanding the long-term stability and performance of the PANI coatings in real-life scenarios, where they may be exposed to elevated temperatures.

Results and discussion

Figure 2a illustrates the cyclic voltammograms obtained during the electrodeposition of PANI coatings (S1) onto the 316L stainless steel substrate using a low scan rate in 10 cycles. The voltammogram displays three distinct peaks observed at approximately 0.2 V, 0.6 V, and 1.1 V. According to [20], peak A corresponds to the partially oxidized emeraldine state of PANI, indicating the formation of radical cations. Peak B represents the fully oxidized form of PANI, known as pernigraniline, while peak C corresponds to the degradation of the radicals into benzoquinone during the polymerization process. The electro-polymerization of aniline generally involves four steps [21]:

- 1- Protonation of the aniline monomer in an acidic environment, leads to the formation of free radicals.
- 2- Formation of dimers.
- 3- Formation of oligomers and the PANI film.
- 4- Growth of the polyaniline film.

Upon repeating the potential scans, the observed increase in the oxidation and reduction peak heights indicates successful deposition of polyaniline onto the stainless-steel substrate and an increase in the film thickness. To investigate the influence of the potential window on the polymerization process, another coating with a different potential window was deposited on the steel surface. Figure 2b presents the cyclic voltammograms during the electro-polymerization of the monomer for the first and second cycles. The peak observed at 1.1 V is attributed to the oxidation of the steel substrate and the formation of a passive layer. The current density decreases in subsequent cycles due to the formation of a more pronounced passive layer. Figure 2c demonstrates the cyclic voltammograms for the subsequent cycles of PANI coating (S2).

To estimate the thickness of the film formed on the surface, the following empirical formula was utilized [22]:

$$d = \frac{Q_a M_w}{zFA\rho} \quad (2)$$

where Q_a represents the amount of charge transferred from the leucoemeraldine to the emeraldine state, M_w

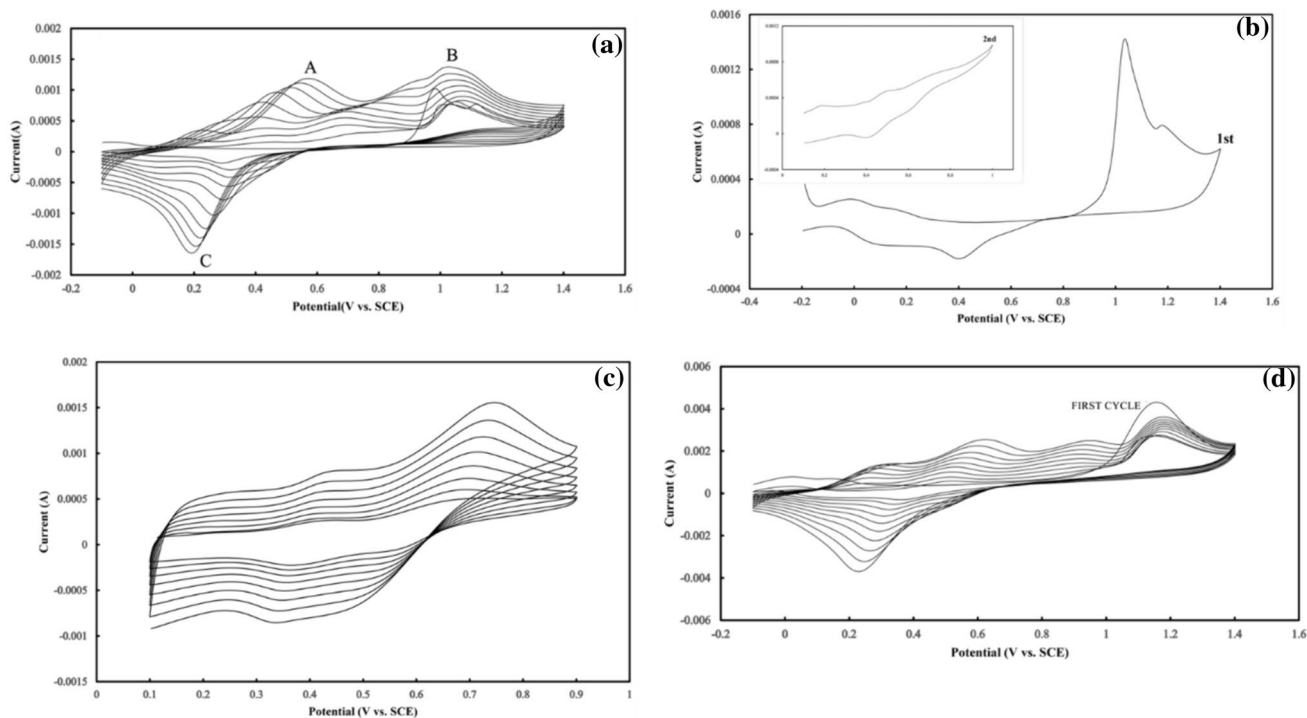


Figure 2 Cyclic voltammetry for PANI coating in 0.1M aniline and 0.1M H₂SO₄.

is the molecular weight of aniline, z is the number of electrons/aniline unit (0.5), A is the electrode area, ρ is the specific density of aniline, and F is Faraday's constant. It is important to note that this formula does not account for factors such as porosity and counter-ion volume, therefore providing only an estimated thickness [23]. According to this formula, the estimated thicknesses of S1 and S2 were 7.7 μm and 8 μm , respectively. It can be observed that the thickness of the coating does not vary significantly between the two samples, with the main difference lying in the degree of adhesion and uniformity.

Figure 2d presents the cyclic voltammograms obtained during the electrodeposition of PANI coating at a high scan rate of 50 mV/s. The maximum current density is observed in the first sweep, while the current density of subsequent cycles is lower than that of the initial sweep. This behavior indicates a restricted growth of the polyaniline film on the electrode surface. The higher scan rate limits the opportunity for polymer chains to effectively join, resulting in a less developed and less uniform film formation. Conversely, when the scan rate is lower, the film formed on the surface tends to exhibit improved homogeneity and uniformity.

In Fig. 3, the FTIR spectra of the PANI thin film are depicted. The peak observed at approximately 1562 cm^{-1} and 1469 cm^{-1} corresponds to the C–C bonds present in the benzenoid and quinoid rings of PANI. Additionally, characteristic vibrations of the C–N bonds are observed at 1300 cm^{-1} , 1243 cm^{-1} , 1180 cm^{-1} , 1051 cm^{-1} , and 1010 cm^{-1} . The peaks at 855 cm^{-1} , 850 cm^{-1} , and 580 cm^{-1} represent the vibrations of the C–H bonds. The FTIR analysis results align well with the findings reported in [24, 25] where similar peaks were observed.

To assess the corrosion behavior, the specimens were immersed in a 1M H₂SO₄ solution for various durations (1, 24, 48, and 72 h), and electrochemical impedance spectroscopy (EIS) measurements were conducted. The EIS data obtained for both uncoated and coated steels was fitted using the equivalent circuit shown in Fig. 4. ZSimpWin 3.30 software was employed for this purpose. In the equivalent circuit, R_s represents the solution resistance between the reference and working electrodes, CPE_1 represents the constant phase element of the coating, R_f denotes the surface film resistance, R_{ct} represents the charge transfer resistance, and CPE_2 corresponds to the constant phase element of the double layer. The constant phase

Figure 3 FTIR spectra of PANI.

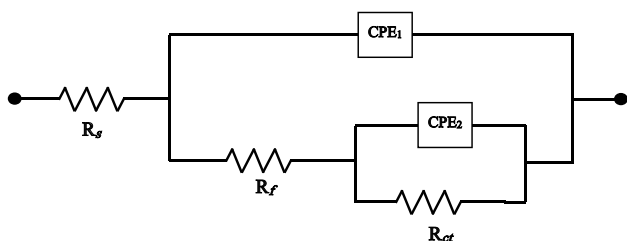
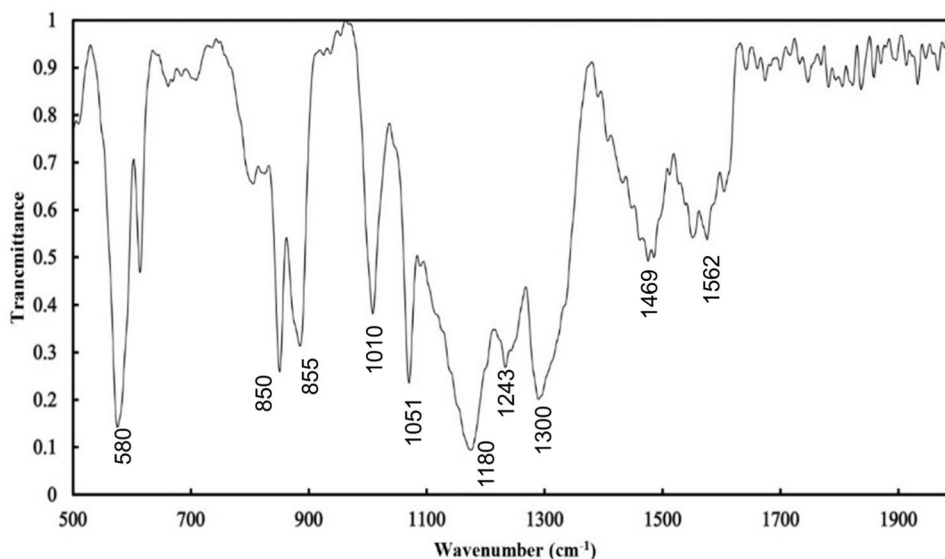


Figure 4 Electrical circuit used to simulate the EIS results.

element (CPE) was utilized in the impedance representation, defined by Eq. (3):

$$Z(Q) = Y_0^{-1} (j\omega)^{-n} \tag{3}$$

Here, Y_0 denotes the CPE constant, ω represents the angular frequency (in rad/s), $j^2 = -1$ is the imaginary number, and n represents the CPE exponent [26]. For the bare steel sample, the equivalent circuit reflects the electrochemical system in which a metal with a porous coating is subjected to ongoing corrosion. It is expected that the behavior of the system will be influenced by the immersion time and the occurrence of pitting corrosion on the surface of the steel.

The Nyquist plots of uncoated stainless-steel specimens immersed in a 1M H₂SO₄ solution are presented in Fig. 5a. After 24 hrs of immersion, there was an increase in the charge transfer resistance (R_{ct}), indicating a decrease in the corrosion rate. This behavior can be attributed to the formation of a

passive layer on the substrate, which acts as a protective barrier against corrosion. However, with prolonged exposure, the passive layer may eventually break down, allowing corrosive agents to penetrate through and leading to severe corrosion of the steel surface. Figure 5b displays the Nyquist plots of the PANI-coated specimens (S_1). Over time, as corrosive agents penetrate the coating, the corrosion reaction initiates at the metal/polymer interface. This interface becomes critical in determining the overall corrosion resistance of the coating.

Over time, the penetration of corrosive agents into the holes or defects in the PANI coating establishes a galvanic coupling between the metal substrate and the polymer. This phenomenon, known as the ennoblement of defects by polyaniline, is illustrated in Fig. 6 [27]. The deliberate removal of a portion of the coating creates a defect, leading to the initiation of corrosion reactions shortly after the ingress of electrolyte into the hole. As a result, cathodic potential shift occurs, causing metal dissolution, while the reduction of the polymer takes place. Consequently, the positive charge accumulated in the polymer is transferred to the defect, thereby maintaining it within the passive region.

Figure 7 presents the standard polarization curve of stainless steel, illustrating two distinct regions: the active region and the passive region, which are separated by a critical passivating current density (i_{crit}). It is crucial to maintain the potential within the passive region to prevent corrosion. Achieving this

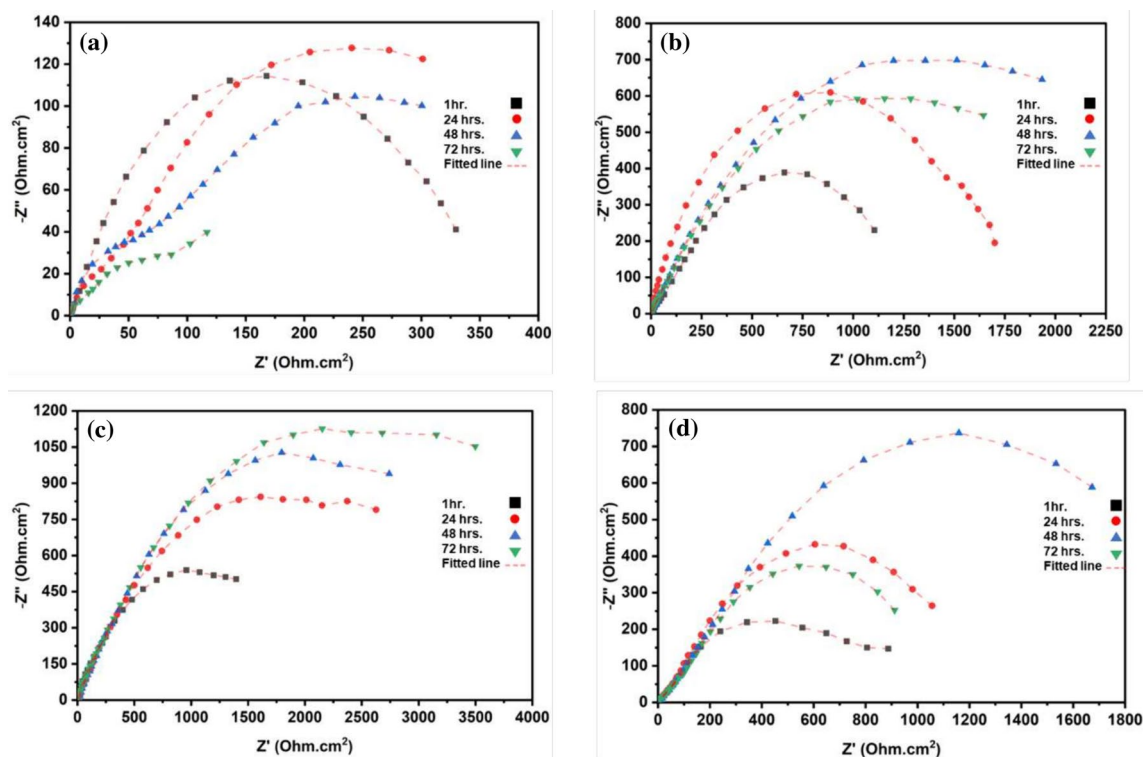


Figure 5 Nyquist plots of the impedance spectra for samples **a** bare, **b** S1, **c** S2 and **d** S3.

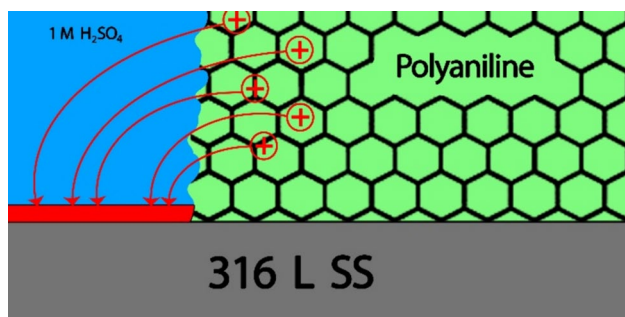


Figure 6 Idea of the defect protection by the conductive polymers.

can be accomplished by applying an anodic current greater than i_{crit} , which effectively shifts the potential of the stainless steel to the passive region. The reduction of polyaniline can serve as a source of current for this purpose.

After 72 hrs. of immersion, the charge transfer resistance observed in the Nyquist curve decreases due to the penetration of the corrosive solution into the substrate. As the immersion time increases, a greater amount of the solution infiltrates the coating, creating pathways for corrosive agents. In Fig. 5c, the

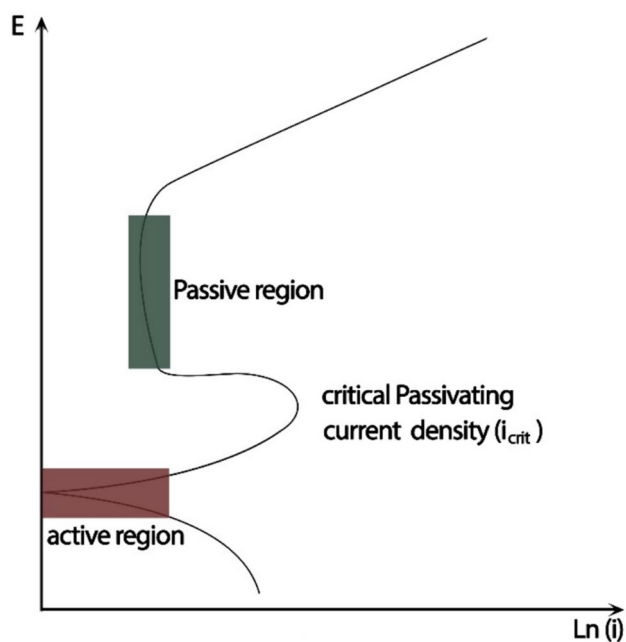


Figure 7 Standard polarization curve of stainless steel.

Nyquist plots of PANI coating (S_2) are shown. Coatings synthesized under these conditions and deposited on the steel surface are expected to exhibit high

corrosion resistance due to the formation of a uniform and low-porosity coating. A less porous coating restricts access of water and other corrosive agents to the steel surface, while polyaniline can effectively passivate defects. Analysis of the Nyquist curves and simulation-derived parameters presented in Table 3 indicate that the coating synthesized within a narrower potential window exhibits higher corrosion resistance. Figure 5d demonstrates the Nyquist plots of the PANI coating synthesized at a high scan rate (S₃). As previously explained, a lower scanning speed allows for the joining of polyaniline chains, resulting in a more regular and structured arrangement of the chains.

The corrosion parameters determined from the Nyquist plots are listed in Table 3, including the roughness coefficient (n), protection efficiency (η), and charge transfer resistance (R_{ct}). In an ideal case, n would equal 1, and the Nyquist plots would appear as perfect semicircles. However, in practice, n is typically less than 1. A decrease in the roughness coefficient indicates an increase in the corrosion rate [28]. The efficiency of protection (η) was calculated using the following equation:

$$\eta = \frac{R'_{ct} - R_{ct}}{R'_{ct}} \times 100 \tag{4}$$

where R'_{ct} and R_{ct} is the charge transfer resistance of coated and bare steel, respectively.

To calculate the corrosion rate (Mpy) at the first corrosion current obtained from Stern-Geary formula [29]:

$$i_{corr} = \frac{0.025}{R_{ct}} \tag{5}$$

Then following formula was used to calculate the corrosion rate in Cm/s:

$$CR = \frac{iM}{ZFD} \tag{6}$$

where i is current density (amps/cm²), M is atomic weight (g/mol), Z is number of transferred electrons, F is Faraday constant and D is density (g/cm²). Following equation was employed for convert to Mpy:

$$1.242 \times 10^{10} \times CR = Mpy \tag{7}$$

According to the standard classification corrosion rate that are given in Table 4, corrosion rates of the samples were compared.

Figure 8 depicts scanning electron micrographs of bare steel and PANI coating samples after 72 h of immersion in a 1M H₂SO₄ solution. In Fig. 8a, the surface of the bare steel exhibits substantial damage caused by the aggressive attack of corrosive agents. The absence of a protective polyaniline coating allows for easy penetration of the corrosive agents, resulting in corrosion of the steel surface. Figure 8b displays the SEM image of PANI coating (S₁) after 72 hrs. of immersion. The image reveals the presence of significant cracks and a non-compact structure within the coating. As previously explained, the infiltration of the electrolyte into these coating defects leads to the formation of a galvanic couple between the PANI and the steel substrate. Consequently, the damaged regions of the substrate where the coating

Table 3 Impedance parameters of bare and coated steels in 1M H₂SO₄

Time(h)	Bare		S ₁			S ₂			S ₃			
	n	R _{ct} (Ω)	n	Rct(Ω)	η (%)	n	R _{ct} (Ω)	η (%)	n	R _{ct} (Ω)	η (%)	
1	0.73	352	–	0.80	1404	74	0.83	1424	75	0.78	895	60
24	0.74	477	–	0.82	1712	72	0.82	2109	77	0.80	1322	63
48	0.76	453	–	0.82	2981	84	0.87	2845	84	0.82	2187	79
72	0.44	172	–	0.83	2583	93	0.85	3054	94	0.80	1131	84

Table 4 Standard classification corrosion rate [30] and The Mpy of the samples in 1M H₂SO₄

Mpy	< 1	1–5	5–20	20–50	50–200
Description	Excellent	Top	Good	Moderate	Poor
Sample	–	S1	S2	S3	Bare
Mpy	–	4.4	3.7	10.1	67.1

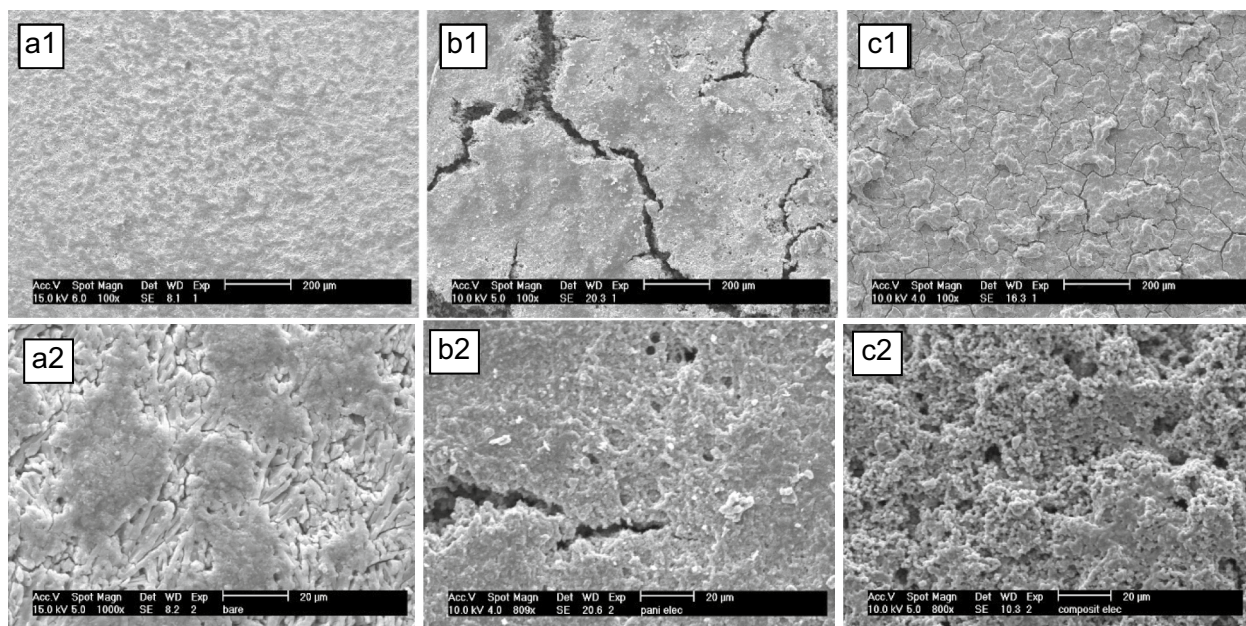


Figure 8 Scanning electron micrograph of **a1**, **a2** bare, **b1**, **b2** S1 and **c1**, **c2** S2.

is compromised undergo passivation, providing some level of protection.

Figure 8c presents the SEM image of PANI coating (S_2) after 72 hrs. of immersion. This figure serves to validate the influence of the potential window used during the polymerization process on the coating's uniformity. Notably, this coating exhibits a more tightly packed and interlocked structure of PANI chains. It is essential to consider the presence of an interlocking and uniform structure within the coating, as it plays a crucial role in ensuring its optimal protective performance. It is important to note that while the observations in the SEM images provide valuable insights, additional quantitative data and analysis would further enhance the understanding of the coating's performance and its ability to withstand corrosion under prolonged immersion.

The thermal stability of PANI was evaluated using thermogravimetric analysis (TGA), and the results are presented in Fig. 9. The TGA curve specifies that PANI experiences thermal degradation at a temperature of approximately 325 °C. As reported in the literature [31], the TGA analysis reveals a three-stage decomposition pattern for PANI. The first stage of weight loss observed in the TGA curve corresponds to the dehydration process, during which PANI undergoes the removal of moisture content. This initial weight loss is attributed to the elimination

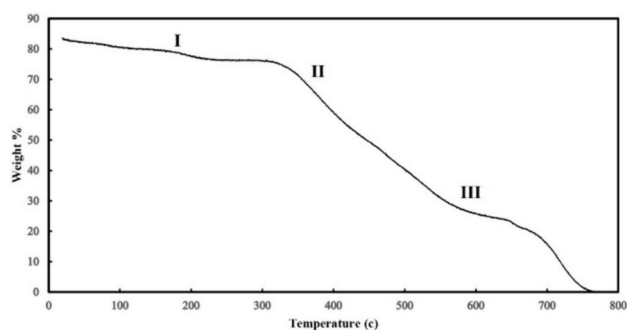


Figure 9 Thermogravimetric analysis curve of PANI.

of water molecules associated with the polymer. The second stage involves the loss of the dopant from PANI. Dopants are typically added during the polymerization process to enhance the electrical conductivity and stability of PANI. The release of these dopant molecules contributes to a further decrease in weight. The final stage of decomposition in the TGA curve corresponds to the breakdown of the polymer chain itself. At this stage, the PANI polymer undergoes thermal degradation, resulting in the fragmentation and decomposition of the polymer structure. By conducting TGA analysis, the thermal stability of PANI can be assessed, providing insights into its performance and suitability for various applications. The observed decomposition pattern in the TGA curve highlights the dehydration process, dopant

loss, and polymer chain degradation as significant factors contributing to the thermal behavior of PANI.

The findings of this study provide valuable insights into the development of effective strategies to protect stainless steel from corrosion in acidic environments. By utilizing electrochemical deposition of polyaniline coatings, it is possible to enhance the corrosion resistance of 316L stainless steel, thereby extending its lifespan and reducing maintenance costs. This research has practical implications in various industries, such as chemical processing, oil and gas, and marine applications, where stainless steel is commonly exposed to acidic environments. Implementing the findings of this study can lead to improved durability and reliability of stainless steel components, ensuring their optimal performance and safety in real-life scenarios.

Conclusion

In conclusion, this study investigated the electrochemical deposition of polyaniline (PANI) coatings on 316L stainless steel to enhance its corrosion resistance in acidic environments. The successful polymerization of PANI onto the stainless-steel substrate was confirmed through cyclic voltammetry with 0.1 M aniline in 0.1 M H₂SO₄ solution, with an increase in film thickness observed with repeated potential scans. Fourier transform infrared spectroscopy (FTIR) analysis revealed characteristic bonds present in PANI, further confirming the successful deposition.

The corrosion behavior of the coated stainless steel was assessed using electrochemical impedance spectroscopy (EIS) in 1M H₂SO₄. The Nyquist plots obtained from the EIS showed that the corrosion resistance of the PANI coating improved significantly with a decrease in scan rate and by limiting the upper potential, especially during longer exposure times. The Nyquist plots of S₂ exhibited a 1.18 times larger diameter than S₁ and a 2.7 times larger diameter than S₃ after 72 h of immersion. This indicates superior corrosion resistance of the coating synthesized within a narrower potential window and at a lower scan rate. The high scan rate in S₃ hinders effective polymer chain joining, resulting in less developed and uniform film formation. In contrast, the lower scan rate in S₂ allows sufficient time for polymer chains to join and form a uniform coating. Additionally, comparing S₁ and S₂, revealed that the first cyclic voltammetry of S₂ occurred within a wider potential window. This

wider range promoted the formation of a uniform passive layer on the steel, enhancing corrosion resistance compared to S₁.

Scanning electron microscopy (SEM) images confirmed the presence of corrosion damage on the bare steel surfaces, while the PANI coating exhibited cracks and a non-compact structure. However, the presence of an interlocked and uniform structure within the PANI coating was observed when the potential window during the polymerization process was optimized.

Overall, these findings demonstrated that controlling the deposition parameters and optimizing the electrochemical conditions can lead to significant improvements in the corrosion resistance of stainless steel, and ultimately, providing valuable information for researchers and engineers in developing better strategies for enhancing the durability and performance of stainless steel in acidic environments.

Acknowledgements

Authors would like to thank the editor and respected reviewers for taking their time to review this paper and provide us with their comments.

Author contributions

Mohammad Fatahiamirdehi: writing original draft, data collection and processing, Mohamad Mahani: validation, visualization, Seyyedeh Forough Mirseyed: data collection and processing, Auref Rostamian: review and edit, validation, Mehdi Ostadhassan: methodology, supervision, review and edit, investigation, resources, funding acquisition.

Funding

Open Access funding enabled and organized by Projekt DEAL.

Data availability

Data will be provided upon request from the corresponding author, Dr. Mehdi Ostadhassan.

Code availability

Data will be provided upon request from the corresponding author, Dr. Mehdi Ostadhassan.

Declarations

Conflict of interest Authors declare no competing interest.

Ethical approval Not Applicable.

Open Access This article is licensed under a Creative Commons Attribution 4.0 International License, which permits use, sharing, adaptation, distribution and reproduction in any medium or format, as long as you give appropriate credit to the original author(s) and the source, provide a link to the Creative Commons licence, and indicate if changes were made. The images or other third party material in this article are included in the article's Creative Commons licence, unless indicated otherwise in a credit line to the material. If material is not included in the article's Creative Commons licence and your intended use is not permitted by statutory regulation or exceeds the permitted use, you will need to obtain permission directly from the copyright holder. To view a copy of this licence, visit <http://creativecommons.org/licenses/by/4.0/>.

References

- [1] Sun Y-T, Tan X, Lei L-L, Li J, Jiang Y-M (2021) Revisiting the effect of molybdenum on pitting resistance of stainless steels. *Tungsten* 3:329–337
- [2] Zaarei D, Sarabi AA, Sharif F, Kassirha SM (2008) Structure, properties and corrosion resistivity of polymeric nanocomposite coatings based on layered silicates. *J Coat Technol Res* 5:241–249
- [3] Shen Z, Zhang J, Wu S, Luo X, Jenkins BM, Moody MP, Lozano-Perez S, Zeng X (2022) Microstructure understanding of high Cr-Ni austenitic steel corrosion in high-temperature steam. *Acta Mater* 226:117634. <https://doi.org/10.1016/j.actamat.2022.117634>
- [4] Zhao Y, Shen Z, Wang Z, Zhang K, Gao S, Wu L, Zeng X (2023) Growth kinetics and microstructure characteristics of the Zr-Cr interlayer in a Cr-coated Zry-4 alloy exposed to high-temperature steam. *Corros Sci* 225:111600. <https://doi.org/10.1016/j.corsci.2023.111600>
- [5] Yang C, Wang C, Zhao X, Shen Z, Wen M, Zhao C, Sheng L, Wang Y, Xu D, Zheng Y, Chu PK, Zeng X (2024) Superhydrophobic surface on MAO-processed AZ31B alloy with zinc phosphate nanoflower arrays for excellent corrosion resistance in salt and acidic environments. *Mater Des* 239:112769. <https://doi.org/10.1016/j.matdes.2024.112769>
- [6] Huang W-S, Humphrey BD, MacDiarmid AG (1986) Polyaniline, a novel conducting polymer. morphology and chemistry of its oxidation and reduction in aqueous electrolytes. *J Chem Soc Faraday Trans 1 Phys Chem Condens Phases* 82:2385–2400
- [7] Peng T, Xiao R, Rong Z, Liu H, Hu Q, Wang S, Li X, Zhang J (2020) Polymer nanocomposite-based coatings for corrosion protection. *Chem Asian J* 15:3915–3941
- [8] Liu X-H, Xia Z-D, Zhou H, Yuan B, Li Z, Guo F (2013) Corrosion behavior of different steel substrates coupled with conductive polymer under different serving conditions. *J Iron Steel Res Int* 20:87–92
- [9] Garcia-Cabezon C, Garcia-Hernandez C, Rodriguez-Mendez ML, Martin-Pedrosa F (2020) A new strategy for corrosion protection of porous stainless steel using polypyrrole films. *J Mater Sci Technol* 37:85–95
- [10] Riaz U, Nwaoha C, Ashraf S (2014) Recent advances in corrosion protective composite coatings based on conducting polymers and natural resource derived polymers. *Prog Org Coat* 77:743–756
- [11] Gao F, Mu J, Bi Z, Wang S, Li Z (2021) Recent advances of polyaniline composites in anticorrosive coatings: a review. *Progress Org Coat* 151:106071
- [12] González M, Saidman S (2011) Electrodeposition of polypyrrole on 316L stainless steel for corrosion prevention. *Corros Sci* 53:276–282
- [13] Elkais AR, Gvozdenović MM, Jugović BZ, Grgur BN (2013) The influence of thin benzoate-doped polyaniline coatings on corrosion protection of mild steel in different environments. *Prog Org Coat* 76:670–676
- [14] Gupta DK, Neupane S, Singh S, Karki N, Yadav AP (2021) The effect of electrolytes on the coating of polyaniline on mild steel by electrochemical methods and its corrosion behavior. *Progress Org Coat* 152:106127
- [15] Umoren S, Solomon M (2019) Protective polymeric films for industrial substrates: a critical review on past and recent applications with conducting polymers and polymer composites/nanocomposites. *Prog Mater Sci* 104:380–450
- [16] Xu H, Zhang Y (2019) A review on conducting polymers and nanopolymer composite coatings for steel corrosion protection. *Coatings* 9(12):807

- [17] Rahman S, Abul-Hamayel M, Aleem B (2006) Electrochemically synthesized polypyrrole films as primer for protective coatings on carbon steel. *Surf Coat Technol* 200:2948–2954
- [18] Wang K, Amin K, An Z et al (2020) Advanced functional polymer materials. *Mater Chem Front* 4(7):1803–1915
- [19] Kankare J, Kupila E-L (1992) In-situ conductance measurement during electropolymerization. *J Electroanal Chem* 322:167–181
- [20] Nalwa HS (1997) Handbook of organic conductive molecules and polymers, volume 4, conductive polymers: transport, photophysics and applications
- [21] Le D, Yoo Y, Kim J, Cho S, Son Y (2009) Corrosion characteristics of polyaniline-coated 316L stainless steel in sulphuric acid containing fluoride. *Corros Sci* 51:330–338
- [22] Hasanov R, Bilgiç S (2009) Monolayer and bilayer conducting polymer coatings for corrosion protection of steel in 1M H₂SO₄ solution. *Prog Org Coat* 64:435–445
- [23] Kraljić M, Mandić Z, Duić L (2003) Inhibition of steel corrosion by polyaniline coatings. *Corros Sci* 45:181–198
- [24] Nam N, Kim J, Lee Y, Son Y (2009) Effect of thermal treatment on the corrosion resistance of polyaniline in H₂SO₄–HF acid mixture solution. *Corros Sci* 51:3007–3013
- [25] Trchová M, Šeděnková I, Tobolková E, Stejskal J (2004) FTIR spectroscopic and conductivity study of the thermal degradation of polyaniline films. *Polym Degrad Stab* 86:179–185
- [26] Kamaraj K, Sathiyarayanan S, Muthukrishnan S, Venkatachari G (2009) Corrosion protection of iron by benzoate doped polyaniline containing coatings. *Prog Org Coat* 64:460–465
- [27] Michalik A (2009) Conductive polymers for corrosion protection: a critical investigation. Ph. D. dissertation, Ruhr-Bochum University
- [28] Thompson NG, Payer JH (1998) DC electrochemical test methods. NACE International
- [29] Bonilla A, Argiz C, Moragues A, Gálvez JC (2022) Effect of sulfate ions on galvanized post-tensioned steel corrosion in alkaline solutions and the interaction with other ions. *Materials* 15(11):3950
- [30] Fontana MG (1987) Corrosion engineering, 3rd ed.
- [31] Kamaraj K, Karpakam V, Sathiyarayanan S, Azim SS, Venkatachari G (2011) Synthesis of tungstate doped polyaniline and its usefulness in corrosion protective coatings. *Electrochim Acta* 56:9262–9268

Publisher's Note Springer Nature remains neutral with regard to jurisdictional claims in published maps and institutional affiliations.